

**MULTIAXIAL FATIGUE BEHAVIOUR OF HEAT TREATED 6061  
ALUMINIUM ALLOY**

**by**

**MARINI BT MARNO**

**Thesis submitted in fulfilment of the requirements for the degree of  
Master of Science**

**December 2011**

## **DECLARATION**

**I hereby declare that I have conducted, completed the research work and written the thesis entitled “Multiaxial Fatigue Behaviour of Heat Treated 6061 Aluminium Alloy”. I also declare that it has not been previously submitted for the award for any degree or diploma or other similar title for any other examining body or University.**

**Name of student: MARINI BT MARNO**

**Signature:**

**Date: 20<sup>th</sup> December 2011**

**Witness by**

**Supervisor: ASSOC. PROF. AHMAD BADRI**

**Signature:**

**BIN ISMAIL**

**Date: 20<sup>th</sup> December 2011**

## **ACKNOWLEDGEMENTS**

First and foremost, I want to take this opportunity to express my almost gratitude to my supervisor, Assoc. Prof. Ahmad Badri Ismail, for his constant encouragement, guidance and support. It is his continuous, unwavering support in the past two years that provides a strong motivation and makes me successful. I will enjoy the great benefit of his instructions forever.

I would like to thank Mr. Mohd. Shahid Abd. Jalal for his kind help in mechanical testing. Special thanks to all technicians, Mr. Mohd. Azam Rejab, Mr. Mokhtar Mohamad, Mr. Mohammad Azrul Zainol Abidin, Mr. Abdul Rashid Selamat, Mr. Mohd. Farid Abd. Rahim, Mr. Sharul Ami Zainal Abidin, Pn Fong Lee Lee and Pn Haslina Zulkifli that managed the equipment and help me during my experiment. I gratefully appreciate the help of technician from School of Mechanical Engineering which is Mr. Azhar Ahmad on preparing and machining the specimens.

I warmly thank all friends who gracefully shared their thinking with me and supplied me with helpful information and comments for my research and who make my stay here a pleasant experience. I would also like to express my gratitude to USM Fellowship for supporting my financial during my two years study here.

Finally, I would like to acknowledge all my family for their unconditional love, support, and most of all, their understanding while completing my studies. I would never achieve this without their support.

# TABLE OF CONTENTS

DECLARATION .....	ii
ACKNOWLEDGEMENT .....	iii
TABLE OF CONTENTS .....	iv
LIST OF TABLES .....	viii
LIST OF FIGURES.....	ix
LIST OF SYMBOLS .....	xvi
ABSTRAK .....	xviii
ABSTRACT .....	xix

## CHAPTER 1- INTRODUCTION

1.1	Introduction .....	1
1.2	Problem Statement .....	2
1.3	Objective of Study .....	3
1.3	Scope of Study .....	4

## CHAPTER 2 - LITERATURE REVIEW

2.1	Introduction .....	6
2.2	Fatigue.....	6
2.2.1	Axial Fatigue and Torsional Fatigue.....	7
2.2.2	Axial Torsional Fatigue.....	10
2.3	Fatigue Failure Mechanism.....	13
2.3.1	Fatigue Crack Initiation Mechanism .....	13
2.3.1.1	Crack Initiation Along Persistent Slip Bands (PSBs).....	16
2.3.2	Crack Propagation Mechanism.....	18
2.3.2.1	Crack Growth Modes.....	18

2.3.2.2	Fatigue Crack Propagation Stages .....	19
2.3.3	Fatigue Fracture Appearance .....	23
2.4	Cyclic Deformation Behaviour .....	28
2.4.1	Hysteresis loop analysis .....	30
2.4.1.1	Cyclic Hardening and Softening .....	30
2.4.2	Cyclic Stress-Strain Response .....	33
2.4.3	Cyclic Stress-Strain Curve .....	34
2.5	6061 Aluminium Alloy .....	36
2.6	Fatigue Life .....	37
2.7	Effect Of Heat Treatment On Fatigue Life and Behaviour .....	39
2.8	Solid Versus Tubular Specimen Fatigue Life and Behaviour .....	42

## CHAPTER 3 - MATERIALS AND METHODS

3.1	Introduction .....	45
3.2	Materials.....	45
3.3	Initial Microstructure .....	47
3.4	Specimens .....	47
3.5	Sample Preparation.....	48
3.5.1	Machining.....	48
3.5.2	Heat Treatment and Aging Process.....	50
3.6	Mechanical Testing.....	51
3.6.1	Monotonic Tensile and Torsion Test .....	52
3.6.2	Low Cycle Fatigue Testing .....	52
3.7	Hysteresis Loop and Cyclic Stress-Strain Curve Plot .....	54
3.8	Hardness Testing .....	57
3.9	Macroscopic Analysis.....	58
3.10	Fractography Analysis .....	59

3.10.1	Sample Preparation .....	62
3.10.1.1	Sectioning .....	59
3.10.1.2	Cleaning of Surfaces .....	59
3.10.2	Failure Damage Analysis .....	59

## CHAPTER 4 - RESULTS AND DISCUSSION

4.1	Hardness .....	61
4.2	Monotonic and cyclic axial and torsion deformations .....	65
4.2.1	Monotonic tensile and torsion deformations .....	65
4.2.2	Cyclic axial and torsional deformations .....	69
4.2.2.1	Cyclic Stress-Strain Response .....	69
4.2.2.2	Cyclic Stress-Strain Curve .....	77
4.3	Fatigue life under axial, torsional and axial torsional fatigue loading .....	82
4.3.1	Axial fatigue life .....	82
4.3.2	Torsional fatigue life .....	84
4.3.3	Axial torsional fatigue life .....	86
4.4	Influence of heat treatment on the fatigue behaviour of 6061 aluminium alloy .....	88
4.5	Effect of the specimen dimension on the fatigue life .....	90
4.6	Fracture surface analysis .....	93
4.6.1	Axial Fatigue .....	93
4.6.2	Torsional Fatigue .....	9
4.6.3	Axial Torsional Fatigue .....	111

## CHAPTER 5 - CONCLUSION AND RECOMMENDATION

5.1	Conclusion .....	112
5.2	Recommendation for Future Work .....	114

REFERENCES .....	115
------------------	-----

## APPENDICES

### APPENDIX A

### APPENDIX B

### APPENDIX C

### APPENDIX D

## LIST OF PUBLICATION

## LIST OF TABLES

Table 3.1	Chemical composition of as-received 6061 aluminium alloy	45
Table 4.1	Comparison between experimental and standard Vickers hardness values	64
Table 4.2	Summary of the room temperature monotonic tensile properties of 6061	67
Table 4.3	Summary of the room temperature monotonic torsion properties of 6061 aluminium alloy	67
Table 4.4	Cyclic torsional properties of solid specimen	81
Table 4.5	Cyclic torsional properties of thin-walled tubular specimen	81
Table A-1	Axial fatigue data for solid specimen	
Table A-2	Axial fatigue data for thin-walled tubular specimen	
Table A-3	Torsional fatigue data for solid specimen	
Table A-4	Torsional fatigue data for thin-walled tubular specimen	
Table A-5	Axial-torsional fatigue data for solid specimens	
Table A-6	Axial-torsional fatigue data for thin-walled tubular specimen	



## LIST OF FIGURES

Figure 1.1	Schematic flow chart showing the overall experimental procedures	5
Figure 2.1	Definition of torsional stress and strain in (a) thin-walled tubular specimen and (b) solid specimen	9
Figure 2.2	Cyclic tension and torsion slip planes with maximum shear stress	10
Figure 2.3	Biaxial fatigue cycles: (a) in-phase (proportional) and (b) 90° out-of-phase (non-proportional)	11
Figure 2.4	(a) Schematic of a body under axial and torsional (biaxial) loading and (b) detail of a small section on the surface of the body shown in (a)	12
Figure 2.5	SEM micrographs showing a crack initiation region of 6061-T6 aluminium alloy : (a) a drawing line distribution of fatigue voids at low and (b) high magnifications	14
Figure 2.6	a) Schematic presentations of the normal and shear fatigue stresses in torsion fatigue specimen and b) Schematic presentation of fatigue crack modes under torsional fatigue loading	15
Figure 2.7	Schematic of slip profile during cyclic loading	17
Figure 2.8	Three modes of crack surface displacements Mode I (opening or tensile mode), Mode II (sliding mode), and Mode III (tearing mode)	18
Figure 2.9	Illustration of Stage I and Stage II fatigue crack propagation	20
Figure 2.10	Typical well defined striations of 2024-T3 aluminium alloy	25

Figure 2.11	Possible mechanisms of the formation of fatigue striation (a) Unstressed. (b) Small tensile stress. (c) Maximum tensile stress. (d) Small compressive stress. (e) Maximum compressive stress. (f) Small tensile stress	26
Figure 2.12	SEM images of fatigue fracture surfaces 6082-T6 aluminium alloy: (a) and (c), 6060-T6 aluminium alloy (b) and (d)	27
Figure 2.13	SEM images of 6061 aluminium alloy cyclically deformed at 27°C. (a) Cracking along grain boundaries and a population of voids of varying size in the region of the stable crack growth, (b) macroscopic voids and shallow dimples in the region of unstable crack growth	28
Figure 2.14	Cyclic softening: (a) constant strain amplitude; (b) stress response (decreasing stress level); (c) cyclic stress-strain response	31
Figure 2.15	Cyclic softening: (a) constant strain amplitude; (b) stress response (decreasing stress level); (c) cyclic stress-strain response	31
Figure 2.16	Characterizing parameters of a stress-strain hysteresis loop	32
Figure 2.17	The cyclic stress response curve for 6061-T651 aluminium alloy	34
Figure 2.18	The derivation of the cyclic stress-strain curve from stabilized hysteresis loops of different strain-range tests	35
Figure 2.19	Monotonic and cyclic stress-strain curve: (a) 6082-T6 aluminium alloy, (b) 6060-T6 aluminium alloy	36
Figure 2.20	Schematic representation of engineering fatigue data, S-N curve and stable hysteresis loops at various fatigue lives	38
Figure 2.21	Comparison of fatigue strength of 2014 aluminium alloy (a) as cast and (b) solution heat treated at 510°C for 2 hours then followed by aging at 190°C for 7 hours	42

Figure 2.22	Comparison of solid and thin-walled tube specimen behaviour	44
Figure 3.1	Flow chart of the experiment	46
Figure 3.2	Solid specimen geometry and dimension	48
Figure 3.3	Tubular specimen geometry and dimension	48
Figure 3.4	Machining steps diagram	49
Figure 3.5	Heat treatments process diagram for solid specimen (a) is the solution heat treatment, T4 – specimens and (b) for precipitation hardening, T6 – specimens	50
Figure 3.6	Heat treatments process diagram for tubular specimen (a) is the solution heat treatment, T4 – specimens and (b) for precipitation hardening, T6 – specimens	51
Figure 3.7	Types of mechanical testing involved in this investigation	51
Figure 3.8	Test specimens that have been mounted into the grip of the machine	53
Figure 3.9	Experimental hysteresis loops obtained from (a) software data and (b) experimental calculation	56
Figure 3.10	Superimposed shear stress-strain loops of solid specimen subjected to torsional fatigue loading	57
Figure 4.1	Bar graph represents the average hardness value of as-received and heat-treated 6061 aluminium alloy	63
Figure 4.2	Microstructure of the heat treated T6 specimen showing finely dispersed submicroscopic $Mg_2Si$ precipitate. (Mag: 20 X, Etchant: Graff and Sargent's etchant)	64
Figure 4.3	Monotonic true stress-strain curve for solid specimen	67

Figure 4.4	Monotonic true shear-stress strain curves for solid specimen	68
Figure 4.5	Monotonic true stress versus true plastic strain	68
Figure 4.6	Monotonic true shear stress versus true plastic shear strain	69
Figure 4.7	Shear stress response as a function of number of cycles for solid specimen: (a) 6061 as-received aluminium alloy; (b) 6061-T4 aluminium alloy and (c) 6061-T6 aluminium alloy	72
Figure 4.8	Shear stress response as a function of number of cycles for thin-walled tubular specimen: (a) 6061 as-received aluminium alloy; (b) 6061-T4 aluminium alloy and (c) 6061-T6 aluminium alloy	73
Figure 4.9	Cyclic stress response curve for solid specimen subjected to axial torsional cyclic loading (a) 6061 as-received aluminium alloy; (b) 6061-T4 aluminium alloy and (c) 6061-T6 aluminium alloy	75
Figure 4.10	Cyclic stress response curve for thin-walled tubular specimen subjected to axial torsional cyclic loading (a) 6061 as-received aluminium alloy; (b) 6061-T4 aluminium alloy and (c) 6061-T6 aluminium alloy	76
Figure 4.11	Monotonic and cyclic shear stress strain curve for solid specimen. (a) As-received 6061 aluminium alloy, (b) 6061-T4 aluminium alloy and (c) 6061-T6 aluminium alloy	79
Figure 4.12	Monotonic and cyclic shear stress strain curve for tubular specimen (a) As-received 6061 aluminium alloy, (b) 6061-T4 aluminium alloy and (c) 6061-T6 aluminium alloy	80
Figure 4.13	S-N curve for solid specimens subjected to axial fatigue loading	83
Figure 4.14	S-N curve for thin-walled tubular specimens subjected to axial fatigue loading	83
Figure 4.15	S-N curve for solid specimens subjected to torsional fatigue loading	85

Figure 4.16	S-N curve for thin-walled tubular specimens subjected to torsional fatigue loading	86
Figure 4.17	Fatigue under in-phase axial torsion loading for solid specimen	87
Figure 4.18	Fatigue under in-phase axial torsion loading for thin-walled tubular specimen	88
Figure 4.19	Cyclic stress response curve for as-received and heat treated specimens	89
Figure 4.20	Effect of specimen geometry on fatigue life of specimens subjected to axial fatigue loading	91
Figure 4.21	Effect of specimen geometry on fatigue life of specimens subjected to torsional fatigue loading	92
Figure 4.22	Fatigue life vs equivalent strain amplitude with solid and thin-walled tubular specimen	93
Figure 4.23	Scanning electron micrograph of the axial fatigue fracture surface of the solid specimen subjected to 60% stress from the yield strength and the resultant fatigue life ( $N_f$ ) of 22309 showing: (a) Overall morphology of failure showing crack initiation region and crack propagation direction. (b) Region 1 shows high magnification of crack nucleation site and early crack growth. (c) Region 2 showing shallow dimples. (d) Fine and shallow striation found in stable crack growth region	94

Figure 4.24	Scanning electron micrograph of the axial fatigue fracture surface of the tubular specimen subjected to 60% stress from the yield strength and the resultant fatigue life ( $N_f$ ) of 90722 showing: (a) Overall morphology of failure showing crack initiation region and crack growth region. (b) Region 1 shows high magnification of crack nucleation site and early crack growth. (c) Region 2 shows population of various sizes of voids and dimple. (d) Shallow striation	96
Figure 4.25	Scanning electron micrograph showing two crack initiation sites observed in tubular specimen	97
Figure 4.26	Torsional fatigue surface crack pattern in the failed 6061-T6 aluminium alloy, (a) and (b) crack initiated on the plane of maximum shear and propagated and branched into maximum normal plane	99
Figure 4.27	Schematic of the fatigue crack modes observed under torsional fatigue loading	100
Figure 4.28	Fractograph showing overall appearance of torsional fatigue fracture surface	101
Figure 4.29	Fractograph showing shear dimples fracture surface resulting from torsional fatigue loading	102
Figure 4.30	Fractograph showing (a) slip trace (arrows) on the side of the dimples and (b) dimples with particles lying inside	102
Figure 4.31	Fractograph showing typical ductile striation in torsional fatigue fractures	103
Figure 4.32	Scanning electron micrographs of the torsional fatigue fracture surface subjected to maximum torsional stress showing (a) Overall morphology of fracture surface. (b) Population of voids and dimples at the crack initiation region. (c) Final overload region shows a transgranular surface of flat near featureless fracture	104

- Figure 4.33 Scanning electron micrographs of the axial torsional fatigue fracture surface of the solid as-received 6061 aluminium alloy specimen showing: (a) Overall morphology of fracture surface and crack propagation direction (b) Region 1 shows a population of macroscopic and fine microscopic voids in the region crack initiation and early crack growth. (c) Fracture surface at region 2 shows fine striations reminiscent of local microplastic deformation. (d) Final overload region (Region 3) shows a transgranular surface of flat near featureless fracture 107
- Figure 4.34 Scanning electron micrographs of the axial torsional fatigue fracture surface of the solid 6061-T4 aluminium alloy specimen showing: (a) Overall morphology of fracture surface. (b) Region 1 and 3 shows a population of microscopic voids and dimples. (c) Fracture surface at region 2 shows tire tracks pattern. (d) Final overload region (Region 4) shows a flat near featureless fracture surface 108
- Figure 4.35 Scanning electron micrographs of the axial torsional fatigue fracture surface of the solid 6061-T6 specimen showing: (a) Overall morphology of fracture surface. (b) Region 2 shows void coalescence to form a fine microscopic crack and dimples. (c) Fracture surface at region 3 shows a population of shallow dimples. (d) Final overload region (Region 4) shows a transgranular surface of flat near featureless fracture 109
- Figure 4.36 Scanning electron micrographs of tubular specimen subjected to a higher axial torsion load showing: (a) Overall morphology of fracture surface. Shear lip at the final fracture. (b) Pockets of fine shallow striations. (c) Population of various sizes of dimples and voids. (d) Fine and shallow dimples. (e) Final overload region showing dimples rupture 110

## LIST OF SYMBOLS

$\sigma$	: Axial stress
$F$	: Axial load
$A$	: Cross sectional area
$\tau$	: Shear stress
$r$	: Radius
$J$	: Moment of inertia
$T$	: Torsional load
$t$	: Wall thickness
$\theta$	: Angle of twist
$l$	: Specimen length
$\sigma_y$	: Tensile yield strength
$\tau_y$	: Shear yield strength
$E$	: Elastic modulus
$G$	: Shear modulus
$K$	: Tensile strength coefficient
$K_o$	: Shear strength coefficient
$n$	: Strain hardening exponent for monotonic tensile
$n_o$	: Strain hardening exponent for monotonic torsion
$K_o$	: Cyclic strength coefficient
$n$	: Cyclic strength hardening exponent
$\Delta\sigma$	: Stress range
$\Delta\epsilon$	: Strain range
$\Delta\tau$	: Shear stress range



$\Delta\gamma$  : Shear stress range

$N_f$  : Number of cycles to failure

# **KELAKUAN LESU BERBILANG PAKSI KE ATAS ALOI ALUMINIUM 6061 TERAWAT HABA**

## **ABSTRAK**

Penyelidikan ini bertujuan mengkaji tindak balas spesimen aloi aluminium 6061 yang diterima dan dirawat haba kepada T4 dan T6 yang berbentuk rod dan tiub berdinding nipis terhadap lesu kitaran rendah sepaksi (tegangan-tegangan), kilasan dan gabungan sepaksi dan kilasan. Aloi ini digunakan secara meluas sebagai bahan di dalam aplikasi bidang aeroangkasa, automobil, pesawat udara, dan struktural kerana mempunyai sifat-sifat mekanikal yang hebat seperti berkekuatan tinggi bagi nisbah berat, kemuluran yang tinggi dan lain-lain. Dalam penyelidikan ini, kajian tindak balas dan kelakuan aloi ini terhadap beban kitaran menggunakan tindakbalas tegasan kitaran dan lengkung kitaran tegasan terikan menunjukkan aloi ini mengalami pengerasan kitaran. Analisis terhadap geometri gelung histerisis juga dilakukan untuk menilai kesan pengerasan atau perlembutan. Kesan rawatan haba terhadap hayat lesu dan kelakuan bahan dibincangkan di mana keadaan T6 memberikan hayat lesu yang tinggi. Perbezaan di antara spesimen berbentuk rod di mana wujudnya kecerunan tegasan dengan spesimen tiub berdinding nipis di mana diandaikan keadaan tegasan adalah seragam juga dibincangkan. Hayat lesu bagi spesimen-spesimen telah direkodkan dan ditunjukkan dalam bentuk lengkung S-N di mana aloi dirawat haba T6 mempamerkan hayat lesu tertinggi berbanding aloi seperti yang diterima dan keadaan T4 tanpa mengira jenis pembebanan berkitar yang dikenakan. Retak bermula pada satah ricih maksimum dan kemudian mula merambat bergantung kepada jenis pembebanan berkitar yang dikenakan kepada spesimen. Melalui analisis fraktrografi, jalur panjang yang cetek dan pelbagai saiz lekuk dan lompong diperhatikan semasa perambatan retak manakala rantau beban lampau akhir memaparkan pecah lekuk.

# **MULTIAXIAL FATIGUE BEHAVIOUR OF HEAT TREATED 6061 ALUMINIUM ALLOY**

## **ABSTRACT**

This study is devoted to investigate the response of solid and thin-walled tubular specimen made of as-received and heat treated into T4 and T6 6061 aluminium alloy subjected to axial (tension-tension), torsional and axial torsional low cycle fatigue. 6061 aluminium alloys have been widely used as a candidate material in aerospace, automobile, aircraft and structural application because of their superior mechanical properties such as high strength to weight ratio and good ductility. In this investigation, the response and behaviour of this alloy to the cyclic loading were studied using cyclic stress response and cyclic stress strain curve shows that this alloy exhibits cyclic hardening. The geometry of the hysteresis loops is also being analyzed in order to evaluate the softening and hardening effect. The effects of heat treatment on the fatigue life and behaviour where T6 condition depict higher fatigue life are discussed. The differences in fatigue behaviours and cyclic deformation between solid and round specimens where a stress gradient exist, and thin-walled tubular specimens where a uniform stress state is assumed are also discussed. Fatigue life of the specimens were recorded and presented in the S-N curve and shows that heat treated T6 alloy exhibits higher fatigue life and fatigue strength compared to the as-received and T4 alloy regardless the type of cyclic loading applied. Cracks initiate on the maximum shear plane and then start to propagate depending on the type of cyclic loading that were applied to the specimens. Through fractographic analysis, shallow striations and various sizes of dimples and voids are observed during the crack propagation while the final overload region exhibits dimples rupture.

# **CHAPTER 1**

## **INTRODUCTION**

### **1.1 Introduction**

Engineering materials that have been used in automobile parts, structural components, aerospace industry and others can be subjected during service condition to cyclic stresses and strains which may locally exceed the yield strength of the particular material. Failure due to this fluctuation of stresses and strains is called fatigue which also consists of the formation and crack growth which can eventually cause sudden fracture. Statistics show that a large percentage of mechanical failures are fatigue failure and due to the difficulties to avoid cyclic stresses and strains in many mechanical components in service, an absolute guideline in future development of more fatigue resistant materials must be achieved by fully understanding the fatigue mechanisms in metals and alloys (Jai-Man, 1983; Rostami, 1986).

Axial fatigue, torsional fatigue and multiaxial fatigue are three major parts of fatigue based on the type of loading and resulting state of stress. The difference between these types of fatigue loading is the stress and strain state. In fatigue analysis, it has been found that materials characteristics including microstructure, chemical composition, heat treatment process, and crystallography are several important factors that influence the cyclic behaviour of materials. Loading history which maybe constant amplitude or completely random are also one of the important factors that influence the cyclic behaviour of materials. Also, it has been found that type of materials also give influence to the crack initiation and propagation

directions rather than applied loading itself. Effects of environment also give influence to the fatigue life of particular materials such as temperatures, corrosion and fretting (Fatemi, 1985).

## **1.2 Problem Statement**

Fatigue is the principal cause of premature failure of engineering components and multiaxial fatigue is a type of fatigue failures that normally occur in most engineering components and structure rather than uniaxial fatigue. Although the fatigue failure criterion for uniaxial loading has been well developed for many decades, the criterion for multiaxial loading does not reach a satisfactory level. This is partly due to complex loadings with complex geometrical shapes of engineering components producing a complex multiaxial stress-strain state which depend on the loading path and make it very difficult to define the fatigue behaviour of materials and structures (Pan et al., 1999). Structures such as pressure vessels, gas turbine, nuclear reactors, aircraft, ground vehicles, and engineering components such as rotating disks, axles and crankshafts are among the some common examples.

In literature, however, little information is available regarding the response and behaviour of this material when subjected to multiaxial fatigue loading. Most studies found in multiaxial fatigue in aluminium alloy were focus on other types of aluminium alloy such as 2000 series (Sadeler et al., 2004) and 7000 series (Zhao and Jiang, 2008). Thus, multiaxial fatigue study in 6061 aluminium alloy is interesting because this material is heat treatable so the microstructural and mechanical properties of this alloy can be tailored by heat treatment.

Nowadays, 6061 aluminium alloy have been widely used as a candidate material in aircrafts, aerospace, automotive and automobile industry. In automobile and automotive industry, this situation led to the demand for increasing vehicle safety that becomes a matter of concern (Sánchez-Santana et al., 2008). Fatigue fracture of automobile parts such as shafts has been occurred under combined axial and torsional loading. For structural materials, the fatigue strength is the most important factor to ensure a long-term reliability. In recent years, it is required that materials used in several applications can sustain very high numbers of load cycles without failure because of fatigue failure is catastrophic and caused undesirable losses. Proper fatigue design includes synthesis, analysis, and testing can reduce these undesirable losses (Stephens et al., 2001).

### **1.3 Objective of study**

The objectives of this research are listed below:

- a) To study the cyclic deformation behaviour of 6061 aluminium alloy including cyclic stress-strain curve behaviour and compared to their monotonic stress strain curves.
- b) To determine the cycle for failure to occur for as-received and heat treated 6061 aluminium alloy by using S-N curve.
- c) To study the difference in cyclic deformation and fatigue behaviour of solid specimen where a stress gradient exist, and thin-walled tubular specimen where a uniform stress state is commonly assumed.
- d) To study the response of cyclic axial, cyclic torsion and the combination of both cyclic axial and torsional load (multi-axial) to the morphology of fracture.

#### **1.4 Scope of Study**

In this study, three different fatigue testing were conducted which are axial fatigue, torsional fatigue, and in-phase (proportional loading) combination of the axial and torsional fatigue. All of the testing was held in the room temperature conditions and under low cycle fatigue. Failure analysis and fracture mechanics approach were used to study the response of the material due to fatigue loading. Figure 1.1 illustrates the whole experimental procedures.

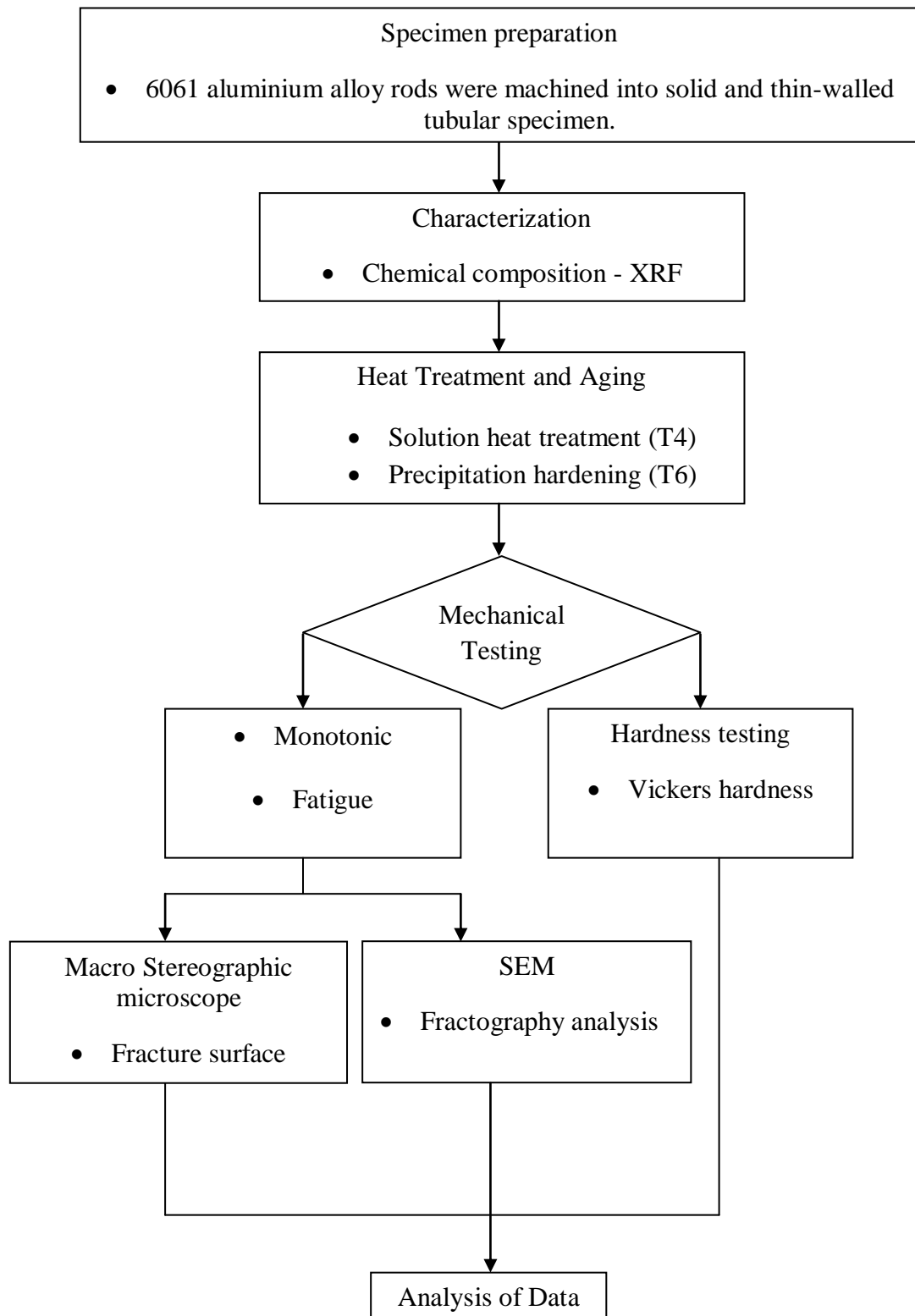


Figure 1.1 Schematic flow chart showing the overall experimental procedures.



## **CHAPTER 2**

### **LITERATURE REVIEW**

#### **2.1 Introduction**

In this chapter, the responses of as-received and heat treated 6061 aluminium alloy due to multiaxial fatigue consists of axial fatigue, torsional fatigue and the combination axial and torsional fatigue are reviewed. The responses consist of cyclic deformation, cycles to failure and fracture appearance due to fatigue failure. S-N curve is used to study the cycles to failure of a 6061 aluminium alloy under different types of loading. The application of the axial torsional fatigue failure and the aluminium alloy in the automotive, aircraft industry and as a structural material are presented in here as well.

#### **2.2 Fatigue**

Fatigue is the phenomenon leading to fracture under repeated or fluctuating stresses with a maximum values less than the tensile strength of the material. It is caused by gross plastic deformation associated with failure and occurs by the initiation and propagation of cracks (Wulpi, 1985).

Due to fatigue, the safety and durability of structures has become more important than before because the sudden failure of complex systems such as nuclear power plants, automobiles, aircraft and pressure vessels may cause many injuries, much financial loss and even environmental damage. Since many of these parts are subjected to repeated multiaxial loadings, fatigue evaluation becomes one of the major considerations in the design of structures. In general, applied loads are

often complex, that is, the corresponding principal stresses are non-proportional, or whose directions change during a cycle of such loadings. Under such loadings, it is very difficult to define the fatigue behaviour of materials and structures (You and Lee, 1996).

Components of machines, vehicles and structures are frequently subjected to repeated loading which may lead to their failure due to fatigue. As can be seen from statistics, a large percentage of mechanical failures are fatigue failure. In addition, the majority of fatigue failure for the components in service is the multiaxial fatigue failure. Therefore, understanding of fatigue failure under multiaxial loading is important to many industrial applications (Pan et al., 1999).

### **2.2.1 Axial Fatigue and Torsional Fatigue**

In general, at the same maximum shear strain/strain amplitude, torsional fatigue has a longer life compared to axial fatigue. This is attributed to the crack face irregularities. The normal tensile stress on the maximum shear plane can open the crack, decrease or eliminate the friction effects, hence assist the crack propagation. This observation leads to the conclusion that only maximum shear plane assists the cracking and should be taken into account. It is also noticed that the ratio of torsional fatigue life to axial fatigue life can vary from one material to another, which means that the friction effect on the fatigue life can vary with materials (Huifang, 2003).

Axial and torsional stresses are derived from the axial load,  $F$ , torsional load,  $T$  and specimen geometry. The axial stress for solid and tubular specimen can be derived as:

$$\sigma = F/A \quad (2.1)$$

where  $A$  is the cross sectional area. The torsional stress for solid specimen can be derived as:

$$\tau = Tr/J \quad (2.2)$$

where  $T$  is the torsional load,  $r$  is the radius and  $J$  is the moment of inertia which is:

$$J = \pi r^4/2 \quad (2.3)$$

For thin-walled tubular specimen, the derivation of torsional stress is based on the assumption that the stress is constant in the cross section of the specimen. The torsional stress is given as:

$$\tau = T/2\pi tr \quad (2.4)$$

where  $T$  is torsional load,  $t$  is wall thickness and  $r$  is the mean radius (from center axis to the mid-thickness of the wall). The torsional strain can be given by:

$$\gamma = r\theta/l \quad (2.5)$$

where  $\theta$  is the angle of twist and  $l$  is the specimen length. Figure 2.1 shows schematically the definition of torsional stress and strain on tubular specimen.

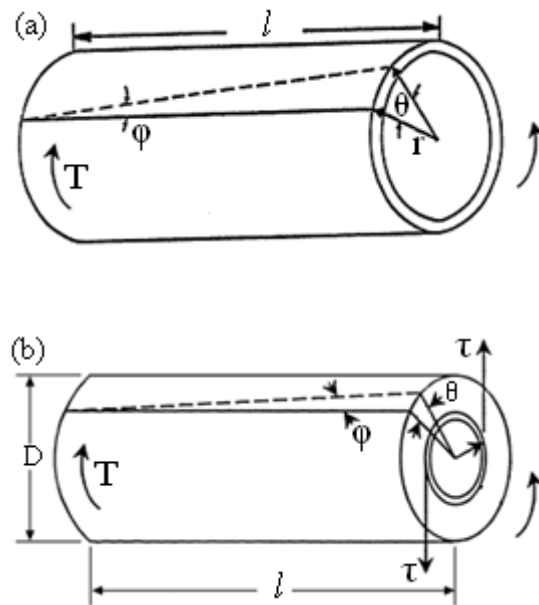


Figure 2.1 Definition of torsional stress and strain in (a) thin-walled tubular specimen and (b) solid specimen (James and Barry, 2009).

The normal and shear stress generated from axial and torsional cyclic loading shown in Figure 2.2. As seen in Figure 2.2, the maximum shear stress under cyclic tension occurs on planes at an angle of  $45^\circ$  with respect to the longitudinal axis. While under cyclic torsion, planes with a maximum shear stress are perpendicular and parallel to the longitudinal axis. An important difference between these two loading systems is that the plane of maximum shear stress in the cyclic tension case also carries a normal stress component ( $\sigma = \tau$ ). However, for cyclic torsion, this normal stress component on the slip plane is zero (Schijve, 2009).

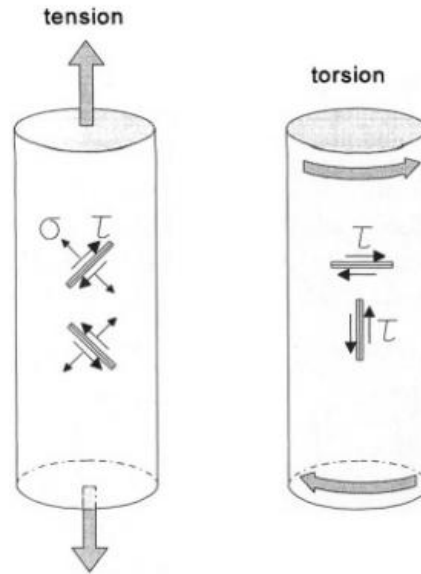


Figure 2.2 Cyclic tension and torsion slip planes with maximum shear stress (Schijve, 2009).

### 2.2.2 Axial Torsional Fatigue

Axial torsional fatigue occurs when the engineering component has been cyclically subjected to both axial and torsional load. Fatigue lives under these combinations of loading conditions can differ significantly from those observed under cyclic uniaxial loading conditions. The multiaxial fatigue problem is more complex compared to uniaxial fatigue due to the complex stress states, loading histories, and different orientations of the initial crack in the components. Numerous attempts have been reported by other researchers in recent decades in order to study and develop multiaxial fatigue damage criteria and fatigue damage modeling. Several reviews and comparisons of existing multiaxial fatigue models can be found elsewhere (Liu and Mahadevan, 2005; You and Lee, 1996; Wang and Yao, 2004). There are two types of loading in axial torsional fatigue which is in-phase or proportional biaxial (multiaxial) fatigue loading and out of phase or non-proportional biaxial (multiaxial) fatigue loading. Figure 2.3 shows the difference

between in phase and  $90^\circ$  out of phase. From the figure we can see that when  $\sigma/\tau$  or  $\varepsilon/\gamma$  is equal to constant the biaxial test is said to be in-phase, or proportional. When there is a phase shift between the axial and torsional cycles, it is said to be out-of-phase or non-proportional and it is also stated that the test is proportional for the purely axial and purely torsional test (Jayaraman and Ditmars, 1989).

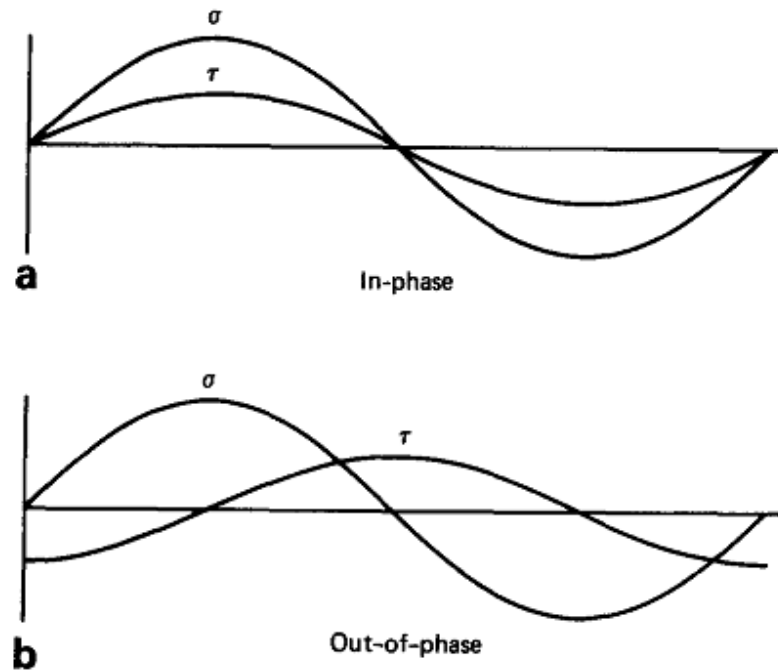


Figure 2.3 Biaxial fatigue cycles: (a) in-phase (proportional) and (b)  $90^\circ$  out-of-phase (non-proportional) (Bannantine et al., 1990) .

In general, plastic deformation occurs when a metallic material have been subjected to a sufficient stress or combination of stress. This deformation is caused by the motion of dislocations which normally called as slip. Slip is likely to occur on those slip systems with the greatest resolved shear stress at any given state of stress. When a cylindrical or tubular body subjected to any combination of axial and torsional load, two of the axes of the principal stresses lie on or parallel to the plane tangential to the surface of the body at any point on its circumference. The third

principal stress is normal to the surface and always has a value of zero. The maximum shear stress acts on a plane whose normal bisects the angle between the directions of the largest and smallest principal stresses. The planes of maximum shear are therefore perpendicular to the surface of the body at all points as shown in Figure 2.4. During proportional loading in axial torsional fatigue test, the principal axes and therefore the maximum shear planes maintain a fixed orientation and only one slip system has the largest resolved shear stress. Under pure axial and pure torsional cyclic loading the orientations of both the principal axes and the maximum shear planes remain fixed with respect to the sample during the course of each cycle (Jayaraman and Ditmars, 1989).

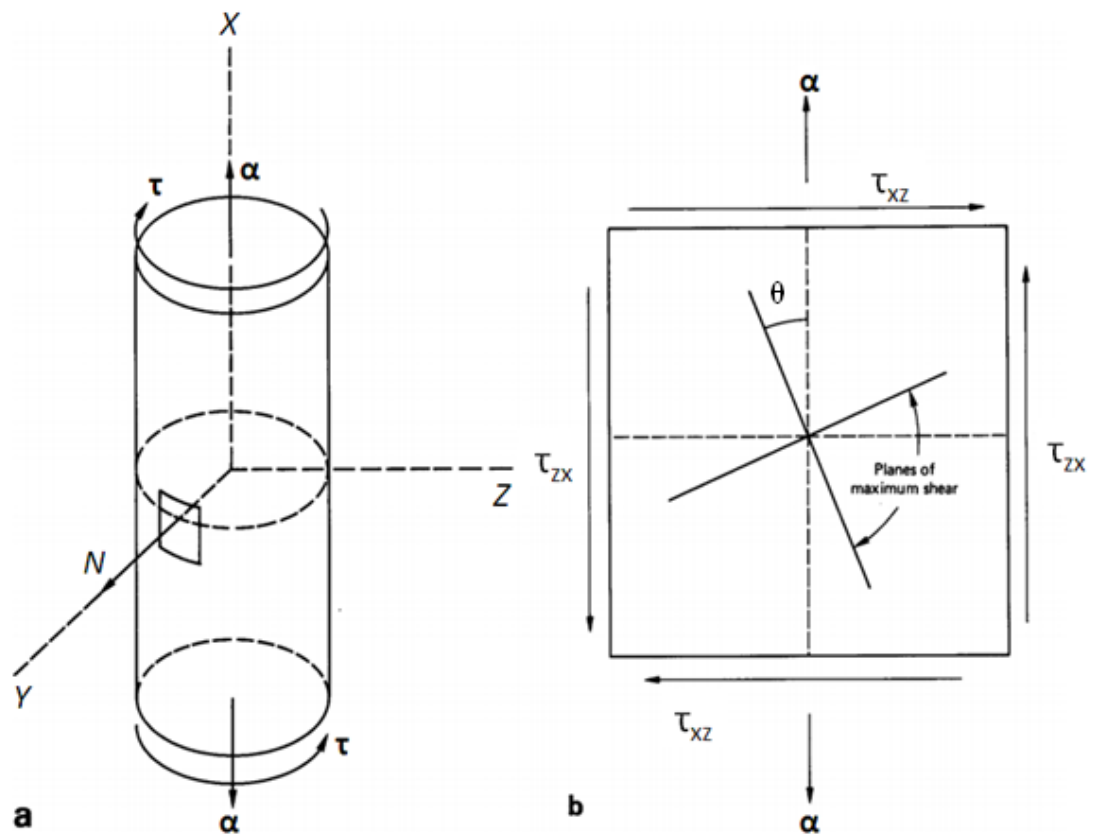


Figure 2.4 (a) Schematic of a body under axial and torsional (biaxial) loading and (b) detail of a small section on the surface of the body shown in (a) (Jayaraman and Ditmars, 1989).

## **2.3 Fatigue Failure Mechanism**

In general, fatigue fracture process is characterized by three stages which the first stage is the initial fatigue damage leading to nucleation and crack initiation. The second stage is a progressive cyclic growth of a crack (crack propagation) until the remaining uncracked cross section of a part becomes too weak to sustain the loads imposed and the final stage is a sudden fracture of the remaining cross section (Liu, 2005; Stephens et al., 2001).

### **2.3.1 Fatigue Crack Initiation Mechanism**

Crack initiation often plays as a major role in fatigue life. In failure analysis, the recognition of location and nature of origin sites of crack initiation is very important. Typically fatigue cracks initiate near the surface where material heterogeneities such as second-phase particles, inclusions, voids and microcracks act as stress concentrators. In aluminium alloy, crack nucleation can occur at intermetallic inclusions which partially contain alloying elements. In general, the inclusions can reduce the ductility of a material due to generating internal voids at large plastic strains but inclusions are not considered to be harmful for the static strength (Schijve, 2009).

Bowles and Schijve (1973) observed that voids created at inclusions by tensile prestrain result in nucleated fatigue cracks of 2024-T3, as did inclusion clusters in unstrained material. Zheng et al. (2011) conducted a fatigue test on AA2524-T34 alloy and found that fatigue crack initiation behaviour of the alloy was influenced by the second phase particles where most of the cracks initiated at the second phase particles or at the interface between particles and the matrix. Fatigue



cracks also initiate near the surface where geometric variations at surfaces exist such as notches, machining marks, surface flaws and others. These stress concentration areas permit local permanent plastic deformation at nominal stresses below material yield strength.

Wang et al. (2006) observed that fracture is initiated from microvoids produced from subsurface facets. Large micro cleavage facets, comprising of a population of micro-voids of a range of sizes, were formed during crack initiation and early growth like shown in Figure 2.5(a) and (b). The expanding voids coalesce to form drawing lines in the cleavage facets. The line-type voids then act as macro-cracks. Fatigue failure starts with the formation, growth, and coalescence of interfacial voids and ends with the propagation of macro-cracks initiated at the base of the voids.

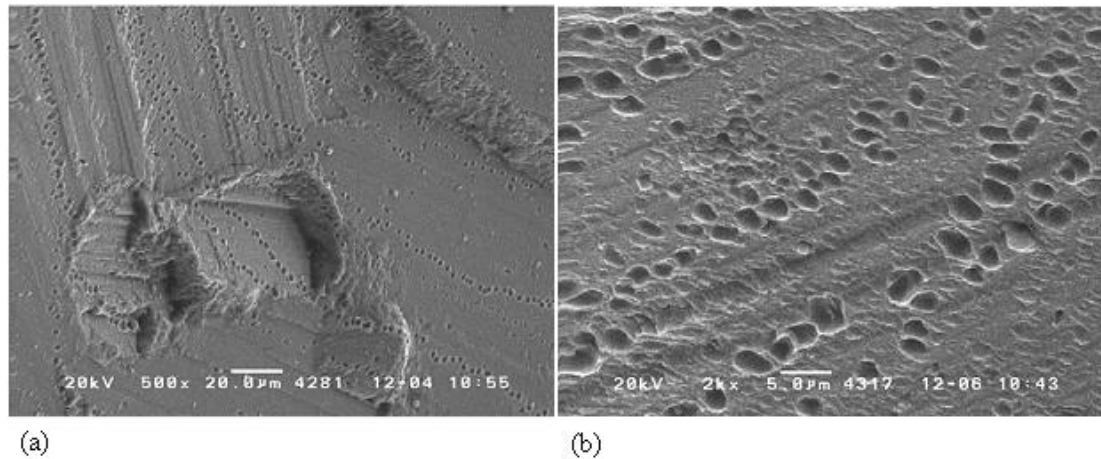


Figure 2.5 SEM micrographs showing a crack initiation region of 6061-T6 aluminium alloy : (a) a drawing line distribution of fatigue voids at low and (b) high magnifications (Wang et al., 2006).

Figure 2.6 shows the normal and shear stress for the specimen that was subjected to torsion cyclic loading. Both tensile and compressive stresses were at  $45^\circ$  to the specimen axis and remained mutually perpendicular. One shear stress component was parallel to the specimen axis, while the other was perpendicular. Under a cyclic torsional loading, fatigue cracks initiated from the surface of the specimen where the shear stress values arrived the highest level. When the fatigue crack initiated, the local stress increases, and different states of stress were formed around the fatigue crack initiation, and local tensile stress on the  $45^\circ$  plane then exceeded the tensile strength of the alloys before the local shear stress exceeded the shear strength of the alloy. Thus, the fracture took place normal to the  $45^\circ$  tensile plane as shown in Figure 2.6(a) (Xue et al., 2008).

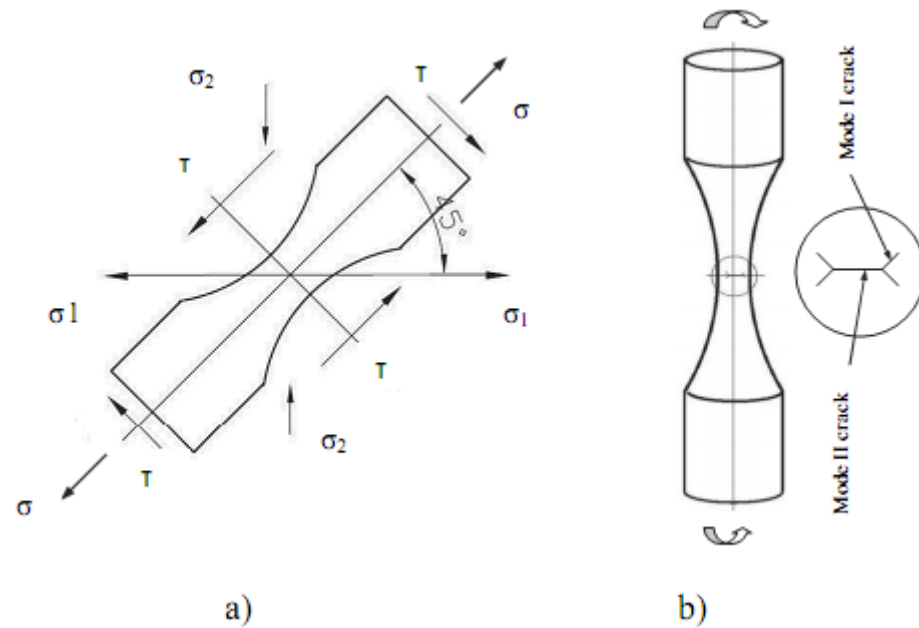


Figure 2.6 (a) Schematic presentations of the normal and shear fatigue stresses in torsion fatigue specimen and (b) Schematic presentation of fatigue crack modes under torsional fatigue loading (Bayraktar et al., 2010).

### **2.3.1.1 Crack initiation along Persistent Slip Bands (PSBs)**

Studies on the mechanism of fatigue crack initiation of single-phase metals which are highly homogeneous shows that the crack also initiates at the surface and it is generally agreed that fatigue cracks are formed by the gradual development of shear bands in the material and the initiation of cracks within the shear bands.

Earlier, Ewing and Humfrey (1903) conducted a rotating bending fatigue test on Swedish iron, of high and very uniform quality. They observed that slip lines develop during the very early stage of fatigue which is after a few reversals of stress and after more reversals of stress, more slip lines appeared. These slip lines changed into wide bands after many reversals and the crystals finally cracked as the widening process continued.

These slip lines are called persistent slip bands (PSBs) and caused by the movement of dislocations. The dislocated PSBs are called intrusion and extrusion, respectively. During the reversal of the stress cycles, some of these bands get pushed in or out, with respect to the surface of the part as shown in Figure 2.7. PSBs are areas that rise above (extrusion) or fall below (intrusion) the surface of the metal due to the movement of dislocation on the crystallography slip planes along the slip directions. The combination of a slip plane and a slip direction is called a slip system. Dislocations movement occurs when resolved shear stress exceeds a critical shear stress on a slip system produce slip steps on the surface of metals. This leaves tiny steps in the surface that serve as stress risers where fatigue cracks can initiate (Huifang, 2003; Liu, 2005).

PSBs represent a type of cyclic plastic strain localization. In single phase materials, the development of persistent slip band associated with the cyclic slip localization has become a fundamental aspect in understanding the mechanism of fatigue crack initiation (Lukáš and Kunz, 2004; Man et al., 2009).

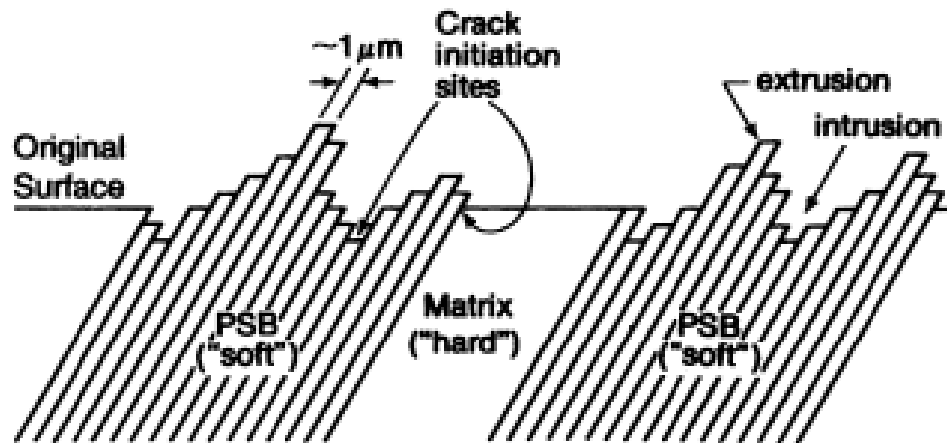


Figure 2.7 Schematic of slip profile during cyclic loading (Liu, 2005).

Baxter and McKinney (1988) studied the growth of slip bands during fatigue of 6061-T6 aluminium alloy and concluded that the persistent slip band initiated within the interior of a grain, often at a site of inclusion or dispersoid. Initially, a persistent slip band appears on the surface in the form of small extrusions. The persistent slip band elongates by the sequential addition of sections of extrusions with spacing about  $1\mu\text{m}$ , and as it does so the initial extrusions become more pronounced. Eventually, microcracks may appear along a well-developed portion of a persistent slip band. Thus, a growing persistent slip band may exhibit a profile ranging from a mature section with pronounced extrusions and microcracks to freshly formed individual small extrusions at the tip. Eventually, when a persistent slip band encounters a major obstacle such as a grain boundary, elongation is terminated but extrusion continues.

Cyclic slip is essential for microcrack nucleation and early microcrack growth. In cyclic tension case, the normal stress tries to open the microcrack and that will enhance the efficiency of the transition from cyclic slip into microcrack growth along the slip band. However, under cyclic torsion this crack opening effect is absent. Microscopic investigations have shown that nucleation in a slip band under cyclic torsion is problematic if the load amplitude is low for example close to fatigue limit. For higher amplitudes above the fatigue limit, microcracks under cyclic torsion are generated which then grow further in a direction to the main principal stress which is  $45^\circ$  with the axis of the bar shown in Figure 2.2 (Schijve, 2009).

### 2.3.2 Crack Propagation Mechanism

#### 2.3.2.1 Crack Growth Modes

There are three basic modes in crack extension mechanism which can cause crack growth. These three modes which are mode I, mode II and mode III are shown in Figure 2.8.

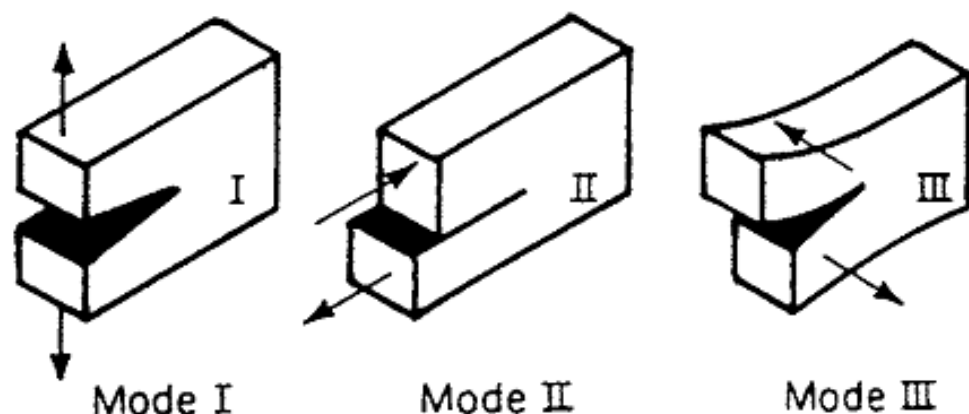


Figure 2.8 Three modes of crack surface displacements Mode I (opening or tensile mode), Mode II (sliding mode), and Mode III (tearing mode) (Bannantine et al., 1990).

Mode I is the opening or tensile mode which is the most common in fatigue. In this mode, crack faces are pulled apart and separate in the direction normal to the crack plane. The corresponding displacements of the crack faces are symmetric with respect to x-y and x-z planes. In-plane shear or sliding mode is called for mode II which the crack surfaces slide over each other. The displacements of crack surfaces are symmetric with respect to x-y and x-z plane. Meanwhile, for mode III crack growth is called anti-plane shear mode or tearing in which crack surfaces are sheared parallel to the crack front. The displacements of crack faces are then anti-symmetric with respect to x-y and x-z plane (Bannantine et al., 1990; Huifang, 2003).

#### **2.3.2.2 Fatigue Crack Propagation Stages**

Stage I crack growth propagation occurs and the propagation or nucleation stage ends in the formation of fatigue surface microcracks. Forsyth (1961) was the first one to observe the three stages of crack growth in uniaxial fatigue and he stated that stage I crack propagation is considered to occur along a crystallographic plane within each grain (Provan and Zhai, 1991).

By uniaxial loading, the maximum shear stress lies in planes oriented at  $45^\circ$  to the direction of applied stress. As the number of slip systems in metals is relatively high, those which are active have orientation near to the maximum shear-stress planes, thus the planes of microcracks are always inclined approximately  $45^\circ$  to the vector of the applied stress. Once initiated, a fatigue crack propagates along high shear stress planes ( $45^\circ$ ), as shown in Figure 2.9, cracks first grow in a shear mode (mode II). This is known as stage I or the short crack growth propagation

stage. Stage I propagation is a shear controlled process. In the course of further cyclic loading, the microcracks grow and link together. A large majority of these microcracks stop propagating quite early and only some achieve a length (or rather depth) greater than a few tens of microns. With increasing length, the growing cracks leave the original near the  $45^\circ$  oriented slip planes and tend to propagate perpendicular to the stress axis. This transition of the crack plane from the active slip plane to a non-crystallographic plane perpendicular to the stress axis is often called the transition from stage I to stage II. The crack propagates until it is decelerated by a microstructural barrier such as a grain boundary, inclusions, or pearlitic zones, which cannot accommodate the initial crack growth direction. Therefore, grain refinement is capable of increasing fatigue strength of the material by the insertion of a large quantity of microstructural barriers such as grain boundaries which have to be overcome in stage I propagation (Klesnil and Lukáš, 1992).

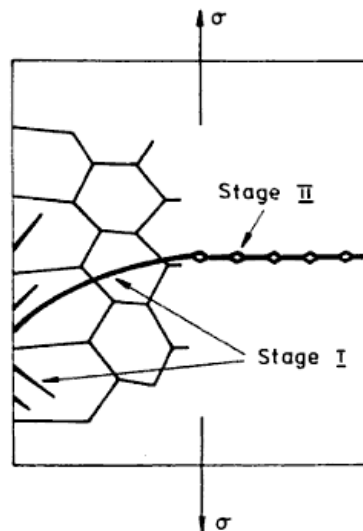


Figure 2.9 Illustration of Stage I and Stage II fatigue crack propagation (Klesnil and Lukáš, 1992).

When the crack orientation becomes perpendicular to the applied stress, it is called stage II crack propagation that is tensile mode (mode I) crack growth. Stage II crack propagation takes over eventually which the crack extension rate increases dramatically. Furthermore, at this point there is also a change in propagation direction to one that is roughly perpendicular to the applied tensile stress. In stage II of fatigue-crack propagation, only one crack usually propagates, all others stop well within stage I. Figure 2.9 also illustrates the stage I and stage II crack propagation. Crack propagation in stage II ends by the fracture of the remaining cross-section. At the very end of fatigue life, stage III crack propagation occurs that more often involves one or more static fracture mechanism. Since crack propagates rapidly in this period, it has little effect on the total life (Huifang, 2003; Klesnil and Lukáš, 1992).

Ohkawa et al. (1997) conducted a fatigue tests on thin-walled tubular specimens of S45C steel under in-phase and out-of-phase axial torsional loadings with different stress ratios. They observed the details on the cracked surface and found that initiation and growth of microcracks are governed predominantly by the shear stress amplitude acting on the crack plane, regardless of the stress ratio or the phase difference. Even in the intermediate cycle regime, the failure crack was formed by the coalescence of many cracks. Frequency of crack coalescence was higher at higher stress ratios. The majority of cracks initiated near the maximum shear planes and then grew changing their orientation to the direction perpendicular to the maximum normal stress. The transition of crack orientation occurred at relatively longer crack lengths for higher stress ratios. An equivalent strain intensity parameter based on strain components acting on the crack plane was found to be



useful for correlating crack growth behaviour under fully-reversed combined loadings at various stress ratios and phase differences.

Bayraktar et al. (2010) conducted a torsional fatigue test on the cast aluminium 2-AS5U3G-Y35 specimens and it shows that crack initiation was always Mode II (Figure 2.6(b)). Fatigue cracks initiated from the centre of the specimen where it was subjected to the maximum shear stress under cyclic torsional loading. When fatigue crack initiation occurs, the local stress increases, and different states of stress form around the initiation site. The local tensile stress on the  $45^\circ$  plane will largely exceed the tensile strength of the alloys before the local shear stress reaches the shear strength of the alloy. Fracture occurred normal to the  $45^\circ$  tensile plane, thus producing a typical torsional fracture surface, as shown in Figure 2.6. They also conducted a torsional fatigue test on AISI52100 steel specimens where fatigue crack initiated from a subsurface inclusion. In this specimen, micro-cracks would grow around the inclusion, thus forming a facet area. When the micro-cracks propagated to the surface of specimen, crack growth occurred in the cyclic tension stress plane at  $45^\circ$  to the axial direction. In this case, shear cracks did not occur. In other words, fracture of the specimen initiated from a subsurface inclusion revealing a completely  $45^\circ$  fracture surface.

Akiniwa et al. (2008) reported on the studies of fatigue strength of oil-tempered Si–Cr steel for valve springs. No specimen showed crack initiation from the interior. Inclusions and granular facet areas could not be observed at the crack initiation site, so that all specimens broke from the surface. Under torsional loading, cracks initiated either perpendicular or parallel to the longitudinal direction of the

specimens. After shear crack, propagation to a crack length of about 30  $\mu\text{m}$ , crack branching and mode I propagation took place.

Bae and Lee (2011) studied the effect of specimen geometry on the low cycle fatigue life of metallic materials states that the most important difference in the solid and hollow specimens in terms of crack propagation is that in the solid specimen, as it propagates, it approaches the middle section of the specimen; however, in the hollow specimen as the crack propagates it approaches the free outer surface. In solid specimen, the crack initiates on the outer surface and propagates toward the middle of the specimen. In contrast to the solid specimen, in the hollow specimen, the crack initiates on the inner surface and propagates toward the outer surface.

### **2.3.3 Fatigue Fracture Appearance**

Usually, a fatigue fracture surface shows macroscopically two different regions which are the fatigue crack propagation region and the final overload region. The final fracture is nearly always a catastrophic event and occurs with almost no plastic deformation. The lack of gross plastic deformation is also a characteristic of the propagation of the fatigue crack. Thus a very distinguishing characteristic of a component which broke due to fatigue loading is that the parts exhibit almost no gross plastic deformation.

A fracture surface that formed during stage II propagation may be characterized by two types of markings termed beach marks and striations. Both of these features indicate the position of the crack tip at some point in time and appear as concentric ridges that expand away from the crack initiation sites. Beach marks and striations are special features commonly associated with fatigue. However, beach mark and striations are not always present on the surface of a fatigue fracture. Each beach mark represents a period of time over which crack growth occurred. These markings are found for components that experienced interruptions during stage II propagation. Beach marks are produced by a change in crack growth condition such as change in environment or stress level or a pause in stress cycling (interruption in service). Therefore, beach marks are not found in most laboratory tests conducted under uniform loading and environmental condition. Moreover, the presence of beach marks is not necessarily conclusive evidence of fatigue fracture, because beach marks may also occur from other types of subcritical crack growth such as stress corrosion cracking. Crack propagation variations in anisotropic or inhomogeneous materials may also occasionally produce beach marks that are difficult to interpret. Fatigue striations are microscopic in size. Each striation is thought to represent the advance distance of a crack front during a single load cycle. Striations width depends on, and increases with, increasing stress range. At this point, it should be emphasized that although both beach marks and striations are fatigue fracture surface features having similar appearances, they are nevertheless different, both in origin and size. There may be literally thousands of striations within a single beach mark (Liu, 2005).